Resonance-enhanced multiphoton-ionization photoelectron spectroscopy of *np* and *nf* Rydberg states of atomic nitrogen

E. de Beer, C. A. de Lange, and N. P. C. Westwood*
Laboratory for Physical Chemistry, University of Amsterdam, Nieuwe Achtergracht 127, 1018 WS Amsterdam, The Netherlands
(Received 20 May 1992)

(2+1) resonance-enhanced multiphoton-ionization photoelectron spectroscopy studies are reported for the metastable $^2D_J^o$ and $^2P_J^o$ nitrogen atomic species presumably produced by photodissociation of the $N_3(X\,^2\Pi_g)$ radical. Two-photon transitions to a multitude of doublet Rydberg states of odd parity are observed in the wavelength range 225.5–294.5 nm. This comprehensive coverage follows all *np* Rydberg states from $n=3$ to the ground-state ionization limit ($^3P_{0,1,2}^e$) with $n=25$ being the highest identifiable. Perturbations are observed around $n=5$ due to an interloping *np* Rydberg state ($n=3$) converging to the first excited ionic limit ($^1D_2^e$). A limited multichannel-quantum-defect theory (MQDT) analysis was performed to estimate the composition of the wave functions in this bound-bound interaction. In addition, *nf* Rydberg states from $n=4$ to 10, and some other weaker quartet states, have also been identified; these, and higher *np* states ($n>8$) show a breakdown of *LS* coupling. Overall, a considerable number of new states have been identified. Photoelectron kinetic-energy scans give information on the ion state distributions from the branching ratios to the $^3P_{0,1,2}^e$ ground and the $^1D_2^e$ and $^1S_0^e$ excited states of N^+; these can be compared to calculated values obtained from the MQDT analysis. Core- and non-core-preserving transitions are observed, and in one case almost complete state selection of excited ($^1D_2^e$) nitrogen atomic ions is observed. Analysis of the Doppler profiles of the atomic transitions provides evidence for the mechanism which is at play in the formation of N metastable states.

PACS number(s): 32.80.Fb

I. INTRODUCTION

In recent work [1], covering the wavelength region 246–286 nm, we have reported preliminary aspects of a (2+1) resonance-enhanced multiphoton-ionization photoelectron spectroscopy (REMPI-PES) [2,3] study of the NH radical obtained from *in situ* photodissociation of hydrazoic acid HN_3. This investigation sought to obtain information on the electronic, vibrational, and particularly, the rotational branching ratios of the ion products, germane to the dynamics of the photoionization process. The primary photodissociation process of the HN_3 precursor has been intensively investigated, with attention focusing on the NH and N_2 internal energy distributions [4–13]. There are many competing channels for photodissociation, especially in the vacuum ultraviolet, where photodissociation leads to the production of electronically excited products, either directly or through secondary processes. NH and N_2 are not exclusive fragments because H and N_3 are also formed as primary products. During the course of these REMPI-PES measurements on NH it became evident that N atoms were also produced, with many two-photon transitions from the $N(^2D_J^o)$ and $N(^2P_J^o)$ metastable states observed. Indeed, the N $2p^2 3p(^2S_{1/2}^o) \leftarrow\!\leftarrow 2p^3(^2D_J^o)$ transition was noted in a previous REMPI wavelength scan of the NH system [14], where the two arrows denote a two-photon transition. N atoms, their energies, oscillator strengths, photoionization cross sections, and reactions are relevant to a variety of processes, especially those in flames [15], the upper atmosphere [16,17], and astrophysical environments [18–20], including theoretical studies related to the OPACITY project, a collaborative effort which aims at calculating accurate atomic data required for opacity calculations [21]. Some experimental and theoretical work on single-photon photoionization of ground and metastable N atoms has been reported [22–26]. Previously, the $^2D_J^o$ and $^2P_J^o$ N atoms have been studied by (2+1) REMPI using as a source microwave discharges in N_2 [27–29]. The observed transitions were $2p^2 3p(2P_J^o) \leftarrow\!\leftarrow 2p^3(^2P_J^o)$ and $2p^2 3p(^2S_{1/2}^o) \leftarrow\!\leftarrow 2p^3(^2D_J^o)$. More recently ground state $N(^4S_{3/2}^o)$ has been detected, also as a product of a microwave discharge, by (2+1) REMPI via the $2p^2 3p(^4D_J^o)$ state [30]. The principal objectives of these studies have been to provide sensitive evaluation of ground and metastable state relative concentrations using selected transitions. The $N(^2D_J^o)$ and $N(^2P_J^o)$ metastables react several orders of magnitude faster with molecular oxygen than do ground state N atoms to form vibrationally excited NO, an important infrared emitter in the upper atmosphere [17]. N atoms have also been monitored by REMPI from neutral channel photodissociation of N_2O [11], NO [31,32], and a rare gas adduct of NO [33], and via an ion dissociation channel of N_2^+ [34].

In this work we report a (2+1) REMPI-PES study of N atoms in which the target species are produced selectively in the $^2D_J^o$ and $^2P_J^o$ states, probably by photodissociation of $N_3(X\,^2\Pi_g)$. In a previous REMPI-PES study of N atoms [35] photoelectron spectra were observed for single-photon ionization of the $2p^2 3p(^2S_{1/2}^o)$ state following absorption of two photons from the $^2D_J^o$ metastable state (produced by photodissociation of N_2O). The sole photoelectron signal at 1.67 eV corresponded to generation of the $^3P^e$ ground-state ion. Analysis of photoelec-

tron angular distributions led to the suggestion of a Cooper minimum near threshold, which was subsequently supported by calculation [36–38]. In that experimental work it was noted that data on high Rydberg states of atomic nitrogen are "quite fragmentary." The present paper sets out to redress this deficiency by presenting results on a multitude of accessible doublet Rydberg states of N I in the region leading right up to the first ionization energy (IE) of 14.534 eV, a region that is traditionally difficult to access. Doublet states of odd parity, specifically the *np* and *nf* series, converging to the ground-state ion, are observed. In addition, some quartet states are weakly detected. Of special interest is the use of REMPI-PES to investigate the resulting ionic state branching ratios since, at the energies used here, it is feasible to select, with two photons, Rydberg states of N I with different ion cores, and photoionize with one additional photon to produce N^+ in its ground ($^3P^e_{0,1,2}$) and/or excited ($^1D^e_2$ and $^1S^e_0$) states. In principle, ionization of a Rydberg level should leave the ion core unaltered, but an interloping series converging to the first excited ($^1D^e_2$) ion perturbs the energy levels around $n=5$, and significantly alters the branching ratios. A specific objective, in the light of recent interest in state-selective chemistry, would be to establish whether or not one could state select N^+ uniquely in ground or excited states. In addition, it is clearly of interest to attempt to investigate the photodissociation mechanism leading to the formation of the $N(^2D^o_J)$ and ($^2P^o_J$) metastables. A preliminary account of this work has been given [39].

II. EXPERIMENT

The experimental setup has been described previously [40]. Briefly, experiments are carried out using the frequency-doubled [employing a β-BaB_2O_4 (BBO) crystal] output of an excimer pumped dye laser system (Lumonics Inc.) operating with a pulse width of ~10 ns and a repetition rate of 30 Hz. The dye laser was operated with the *C*-540, *C*-500, *C*-480, and *C*-460 dyes to provide tunable radiation between 290.3 and 225.5 nm, at a bandwidth of ~0.08 cm^{-1}. The laser output (~150 μJ/pulse) was focused (focal length 25 mm) into the ionization region of a "magnetic bottle" electron spectrometer. A diverging magnetic field (diverging from ~1 T in the ionization region to ~10^{-3} T in the flight tube) allows the kinetic-energy resolved detection of the photoelectrons with ~50% collection efficiency and an energy resolution of 6–8 meV. The original design [41] has been modified to allow the study of reactive and transient species.

Two kinds of experiments are carried out. First, excited states are located by scanning the excitation wavelength while simultaneously detecting the total, or some energy selected fraction of the total, electron current. Second, the laser wavelength can be tuned to a feature of interest and the ejected photoelectrons are then analyzed according to their kinetic energies. As the photoelectron acceptance angle is 2π sr, no angular resolved measurements are possible, and the observed ionic branching ratios are the "true" branching ratios.

The dye laser wavelength was calibrated in the visible using optogalvanic lines of neon, excited in a hollow cathode discharge. Additionally, (2+1) REMPI signals of $N(^2D^o_J)$ and $N(^2P^o_J)$ via known intermediate states provided a confirmation of the calibration [42–44]. The energy scale of the photoelectron spectra was calibrated using (2+1) ionization of Xe at 249.6 nm.

N atoms are produced in the $^2D^o_J$ and $^2P^o_J$ metastable states probably by photodissociating $N_3(^2\Pi_g)$. $N_3(^2\Pi_g)$ is, in turn, generated from photodissociation of HN_3, produced *in situ* by gently heating a solid 5:1 mixture of stearic acid and NaN_3 to ~380 K [1]. Ideally, to study transitions from $N(^2D^o_J, ^2P^o_J)$ over a wide range of energies, photodissociation leading to $N_3(X\,^2\Pi_g)$, and subsequent dissociation to give the target N metastables should occur with little variation in the quantum yield. In the present study, photodissociation and subsequent REMPI are carried out with one laser only. We cannot, therefore, determine the branching ratios either for formation of the neutral metastable N atoms or, indeed, for the two-photon transitions to the intermediate Rydberg states.

III. RESULTS AND DISCUSSION

A. General considerations

In Fig. 1 an energy-level diagram showing several relevant electronic states of N I, and the three lowest cat-

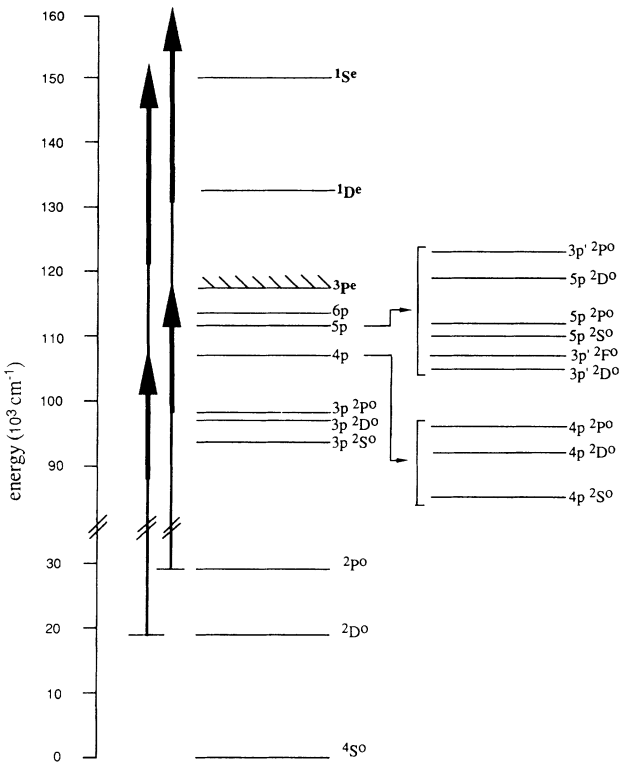

FIG. 1. Energy-level diagram for some of the relevant states of N I and N II. The regions where ($^3P^e$)4*p* and ($^3P^e$)5*p*, as well as the ($^1D^e$)3*p* interloper states are located, are enlarged. The lengths of the arrows indicate the accessible ranges. Note the scale discontinuity between 30 000 and 90 000 cm^{-1}.

ionic states, is depicted, together with some of the transitions to be discussed here. The lowest electronic configuration of the N atom is $1s^2 2s^2 2p^3$. This configuration supports the $^4S^o_{3/2}$ ground state and the $^2D^o_J$ and $^2P^o_J$ metastable states. Removal of an outer electron produces the lowest electronic configuration $(2p)^2$, giving rise to the $^3P^e_{0,1,2}$ ground and $^1D^e_2$ and $^1S^e_0$ excited ionic states.

In the present experiments, two-photon transitions from the $^2D^o_J$ and $^2P^o_J$ metastable states are studied in the wavelength region 290.3–225.5 nm. Strict two-photon selection rules are *even-even, odd-odd,* and $\Delta J = 0, \pm 1, \pm 2$ with $J = 0 \not\leftrightarrow J = 1$. The parity selection rule implies that from the $^2D^o_J$ and $^2P^o_J$ initial states two-photon transitions to the $(2p)^2 np$ and $(2p)^2 nf$ Rydberg states are allowed. Transitions from ground state $^4S^o_{3/2}$ nitrogen atoms were looked for in (3+1) REMPI, but none were observed.

The $2p^3$ valence and the lowest np Rydberg states can best be described in an LS-coupling scheme. In this coupling scheme the additional two-photon selection rules $\Delta S = 0$ and $\Delta L = 0, \pm 1, \pm 2$ with $L = 0 \not\leftrightarrow L = 1$ hold. LS-coupling breaks down for higher members of the Rydberg series, where the ordering of states within one multiplet is no longer governed by electron correlation, but by the spacing between the fine-structure components of the ionization limits ($^3P^e_0$, $^3P^e_1$, and $^3P^e_2$) to which these higher states converge, i.e., by spin-orbit coupling in the ionic state. These higher members of the np series where the Rydberg electron becomes uncoupled from the ion core and the total nf series can best be described in a different coupling scheme. The nf Rydberg electron is nonpenetrating, i.e., the orbital angular momentum ($l = 3$) is greater than the highest orbital angular momentum present in the ionic core. Hence LS coupling is not valid in the nf series even at low n. In an appropriate coupling scheme, $J_c K$ (or $j_c l$) [45], the total angular momentum of the ion core (J_c) is coupled to the orbital angular momentum of the Rydberg electron (l) to form the quantum number K. Finally, the spin s of the Rydberg electron is coupled to give the total angular momentum J. For $(^3P^e)nf$ states, the total orbital angular momentum (L) also tends to be a good quantum number, resulting in a labeling $S[K]_J$, $P[K]_J$, $D[K]_J$, etc.

In the energy range studied, only the two lowest Rydberg states $(^3P^e)3p$ and $(^3P^e)4p$ are accessible with two photons from the $^2D^o_J$ initial state, whereas from the higher lying $^2P^o_J$ initial state the complete Rydberg series converging to the $^3P^e$ limit are within reach at the two-photon level (Fig. 1). These series have previously been reported to $n = 5$ for the doublet states, and to slightly higher principal quantum numbers ($n = 6$–7) for the quartet states [43]. In this study the series are extended to much higher values: to $n \sim 25$ for the np series, before intensity is lost ~ 180 cm^{-1} below the IE.

The $(^3P^e)np$ Rydberg series are perturbed around $n = 5$ by interlopers, namely various configurations of the $(^1D^e_2)3p$ state, the first members of the Rydberg series converging to the lowest excited state of the ion. The perturbations reveal themselves in the shifted line positions in the wavelength scan and in the ionic state branching ratios observed in the photoelectron (PE) spectra. As the perturbations occur at quite low principal quantum numbers, relatively few levels are perturbed and not enough information is available for a full multichannel-quantum-defect theory (MQDT) analysis [18,46–48]. Limited MQDT analyses were, however, performed to roughly estimate the composition of the wave functions affected by the perturbation.

For many of the resonances observed in the wavelength scans photoelectron spectra are recorded in order to assess the ionic state branching ratios. In a (2+1) ionization scheme, one ($^3P^e_{0,1,2}$) to three ($^3P^e_{0,1,2}$, $^1D^e_2$, and $^1S^e_0$) ionic states are energetically accessible, depending on the initial state ($^2D^o_J$ or $^2P^o_J$) and the photon energy. The $J = 0$, 1, and 2 components of the $^3P^e_J$ ionic state should, in principle, be resolved with the available instrumental resolution (~ 6–8 meV). The N atoms are, however, generated in a photodissociation process with significant translational energy. This leads to Doppler broadening of the photoelectron signals of ~ 15 meV, thus obscuring the different J components. Some Doppler broadening is also apparent in the wavelength scans where the atomic transitions show a width of typically 1.2 cm^{-1}.

Photoionization of Rydberg states should, in principle, occur with preservation of the ion core. Core switching can be strong when configuration interaction is important, for instance at the intermediate state level. This will be shown to be true for the members of the $(^3P^e_{0,1,2})np$ Rydberg series which are perturbed by the $(^1D^e_2)3p$ interlopers. In addition, even for unperturbed high $(^3P^e_{0,1,2})np$ Rydberg states, core switching appears to be not negligible, which could be ascribed to configuration interaction in the continuum.

In the following sections the results of this study will be discussed in more detail. First, attention will be focused on the two-photon resonances observed in the wavelength studies from the $^2D^o_J$ and $^2P^o_J$ initial states. Second, the ionic state branching ratios observed in the photoelectron spectra obtained for ionization via the observed resonant states will be discussed.

B. Wavelength studies

1. Transitions from the $^2D^o_J$ initial state

The $^2D^o_{5/2}$ and $^2D^o_{3/2}$ states lie 19 224.464 and 19 233.177 cm^{-1}, respectively, above the $^4S^o_{3/2}$ ground state [43]. Two-photon absorption from these states employing the wavelengths in the range 290.3-225.5 nm reaches excited states $\sim 88\,100$–$107\,900$ cm^{-1} above the $^4S^o_{3/2}$ ground state. Within this energy range the only states of the correct symmetry are the $(^3P^e)3p$ and $(^3P^e)4p$ Rydberg states, the $(^3P^e)4f$ lies higher. In LS coupling the $(^3P^e)np$ Rydberg series consist of five doublet states and eight quartet states. At these low principal quantum numbers LS coupling should still hold, implying that only transitions to doublet states are allowed. Transitions to all doublet states associated with the $(^3P^e)3p$ and $(^3P^e)4p$ configurations are indeed observed in the wavelength scan as strong resonances, except for transitions to the $^2S^o_{1/2}$ states, which are much weaker. As these energy levels have previously been reported [43],

these resonances serve as wavelength calibration, and are not reported here. No transitions to quartet states are observed.

2. *Transitions from the $^2P^o_J$ initial state*

The $^2P^o_{1/2}$ and $^2P^o_{3/2}$ states lie 28 838.920 and 28 839.306 cm^{-1}, respectively, above the $^4S^o_{3/2}$ ground state [44]; the $J=\frac{1}{2}$ and $\frac{3}{2}$ components are not resolved in the wavelength scan. From these initial states, a much more comprehensive series of *np* and *nf* excited states in the energy range 97 700–117 440 cm^{-1} above the $^4S^o_{3/2}$ ground state are accessible by two-photon absorption (Fig. 1), encompassing the complete Rydberg series converging to the $^3P^e_{0,1,2}$ ionic limits (unweighted mean value, 117 314.55 cm^{-1}) [44].

$(^3P^e)nf$ series. From the $^2P^o_{3/2}$ initial state, transitions to all $(^3P^e)nf$ Rydberg states except $G[5]_{11/2}$, $G[5]_{9/2}$, $G[4]_{9/2}$, and $F[4]_{9/2}$ which exceed the maximum change in angular momentum $\Delta J=2$ are allowed. The $(^3P^e)nf$ Rydberg series have previously been reported for $n=4$–6 [43]. In the present experiments these series are observed weakly starting at $n=4$ and are extended to much higher n (~ 10). The observed energy levels and tentative assignments are given in Table I. The experimental line positions agree to within experimental uncertainty with positions calculated on basis of quantum defects, indicating that perturbations are very small.

$(^3P^e)np$ series. Transitions to the *np* Rydberg states are the most prominent and extensive series (up to $n=25$) observed in the present study. As indicated above, in *LS* coupling the $(^3P^e)np$ Rydberg series consist of five doublet states, namely $^2S^o_{1/2}$, $^2P^o_{1/2}$, $^2P^o_{3/2}$, $^2D^o_{3/2}$, and $^2D^o_{5/2}$, and eight quartet states, namely $^4S^o_{3/2}$, $^4P^o_{1/2}$, $^4P^o_{3/2}$, $^4P^o_{5/2}$, $^4D^o_{1/2}$, $^4D^o_{3/2}$, $^4D^o_{5/2}$, and $^4D^o_{7/2}$. Resonances associated with two-photon transitions from the $^2P^o_{1/2,3/2}$ state to all the doublet states show up as very strong resonances in the wavelength scan, apart from transitions to the $^2S^o_{1/2}$ states which are weak. It should also be noted that transitions to the $n=3$ and 4 Rydberg states are much weaker than transitions to the $n=5$ states. This could be due to a sudden decrease in the two-photon excitation or ionization matrix elements; it seems more likely, however, that the dominant photodissociation channel leading to $^2P^o_J$ nitrogen atoms is closed at these lower energies. Possible photodissociation mechanisms will be discussed in a later section.

The $(^3P^e)np$ series have previously been reported only to $n=5$ for the doublet states, and to slightly higher principal quantum numbers ($n=6$–7) for the quartet states [43]. This is due, in part, to the fact that states of odd parity are not accessible by one-photon absorption from the $^4S^o_{3/2}$ ground state. Also, these states are located 14–14.5 eV above the ground state, which makes them difficult to access in conventional one-photon spectroscopy. Figure 2 shows a wavelength scan covering the two-photon energy from 86 750 to 88 500 cm^{-1}, which embraces the *np* series from $n=9$ to 24, and also shows some of the weak *nf* series. The observed *np* transitions are listed in Table II, where the Rydberg states are denoted in *LS* coupling even for high *n*.

For low n ($n=4$–5), as with the $^2D^o_J$ metastable origin, no transitions to quartet states are observed. At $n=6$ very weak features attributable to quartet states are discerned, but only for still higher n (≥ 8) do these states become appreciable in intensity. Assignments have remained very tentative and are not reported. The principal quantum number at which *LS* coupling breaks down can be estimated by comparing the $^4D^o_{5/2}$ and $^2D^o_{5/2}$ energy difference for a given *n* and the $^3P^e_1$ and $^3P^e_2$ energy difference, these being the states to which the quartet and doublet states, respectively, converge. At low *n*, the doublet-quartet splitting (due to electron correlation) is much greater than the $^3P^e_1$ and $^3P^e_2$ energy difference in the ion (due to spin-orbit coupling), so the latter can be treated as a perturbation. Going up in *n*, the ($^4D^o_{5/2}$-$^2D^o_{5/2}$) energy difference converges to the ($^3P^e_1$-P^e_2) splitting, and when this difference decreases to a few times the ($^3P^e_1$-$^3P^e_2$) energy difference, both effects are comparable in strength. Hence spin-orbit coupling can no longer be treated as a perturbation, implying that the *L* and *S* are no longer good quantum numbers from approximately $n=7$ onwards; this is supported by the observation that transitions to quartet states are first weakly observed at

TABLE I. Term values for the observed $(^3P^e)nf$ Rydberg states. Energy levels not previously observed, to the best of our knowledge, are denoted by asterisks.

Term value (cm^{-1})	Assignment
110 349	$4f\ D[3]^o$
110 385	$4f\ G[3[^o$
110 402	$4f\ G[4]^o$
110 404.5	$4f\ D[2]^o$
110 459.5	$4f\ D[1]^o$
110 486	$4f\ F[2]^o$
110 498	$4f\ F[3]^o$
110 501.5	$4f\ F[4]^o$
112 826	$5f\ D[3]^o$
112 869	$5f\ G[3]^o$
112 880	$5f\ D[2]^o$,$5f\ G[4]^o$
112 948	$5f\ D[1]^o$
112 958	$5f\ F[2]^o$
112 967	$5f\ F[3,4]^o$
114 171	$6f\ D[3]^o$
114 216	$6f\ G[3]^o$
114 222	$6f\ D[2]^o$,$6f\ G[4]^o$
114 296	$6f\ D[1]^o$
114 302	$6f\ F[2]^o$
114 307	$6f\ [3,4]^o$
114 981*	$7f\ D[3]^o$
115 033*	$7f\ D[2]^o$,$7f\ G[4]^o$
115 108*	$7f\ D[1]^o$
115 115*	$7f\ F[2,3,4]^o$
115 508*	$8f\ D[3]^o$
115 558*	$8f\ D[2]^o$,$8f\ G[4]^o$
115 640*	$8f\ F[2,3,4]^o$
115 871*	$9f\ D[3]^o$
115 919*	$9f\ D[2]^o$,$9f\ G[4]^o$
116 001*	$9f\ F[2,3,4]^o$
116 177*	$10f\ D[2]^o$
116 258*	$10f\ F[2,3,4]^o$

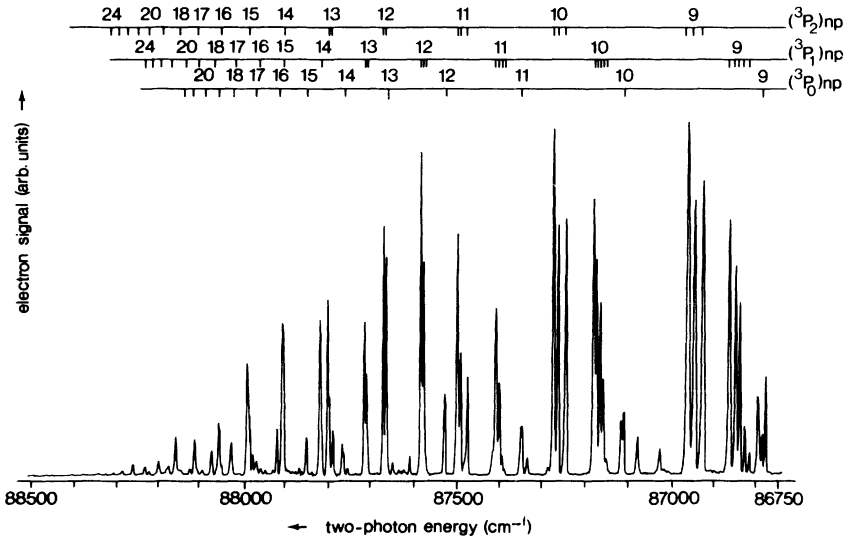

FIG. 2. Wavelength scan (not corrected for dye efficiency curve) covering the *np* series from $n=9$ to 24. The limits to which the individual components converge, are indicated. Weak features at ~87 000–87 100 and ~87 350 cm^{-1} are assigned to the *nf* series.

TABLE II. Term values for the observed ($^3P^e$)*np* Rydberg states. Energy levels not previously observed, to the best of our knowledge, are denoted by asterisks.

Term values (cm^{-1})	Assignment	Term values (cm^{-1})	Assignment
96 788	$3p\ ^2D^o_{3/2}$	116 023*	$10p\ ^2D^o_{3/2}$
96 864	$3p\ ^2D^o_{5/2}$	116 087*	$10p\ ^2P^o_{1/2}$
97 770	$3p\ ^2P^o_{1/2}$	116 106*	$10p\ ^2D^o_{5/2}$
97 806	$3p\ ^2P^o_{3/2}$	116 117*	$10p\ ^2P^o_{3/2}$
107 183	$4p\ ^2D^o_{3/2}$	116 250*	$11p\ ^2D^o_{3/2}$
107 253	$4p\ ^2D^o_{5/2}$	116 317*	$11p\ ^2P^o_{1/2}$
107 588	$4p\ ^2P^o_{1/2}$	116 333*	$11p\ ^2D^o_{5/2}$
107 628	$4p\ ^2P^o_{3/2}$	116 341*	$11p\ ^2P^o_{3/2}$
110 521[a]	$3p'\ ^2D^o_{3/2}$	116 423*	$12p\ ^2D^o_{3/2}$
110 545[a]	$3p'\ ^2D^o_{5/2}$	116 489*	$12p\ ^2P^o_{1/2}$
110 711[a]	$3p'\ ^2F^o_{5/2}$	116 506*	$12p\ ^2D^o_{5/2}$
110 715[a]	$3p'\ ^2F^o_{7/2}$	116 512*	$12p\ ^2P^o_{3/2}$
111 199	$5p\ ^2P^o_{1/2}$	116 555*	$13p\ ^2D^o_{3/2}$
111 213	$5p\ ^2P^o_{3/2}$	116 628*	$13p\ ^2P^o_{1/2}$
111 853	$5p\ ^2D^o_{3/2}$	116 641*	$13p\ ^2P^o_{3/2}$
111 907	$5p\ ^2D^o_{5/2}$	116 659*	($^3P_1$)14*p*
112 294[a]	$3p'\ ^2P^o_{1/2}$	116 746*	($^3P_2$)14*p*
112 320[a]	$3p'\ ^2P^o_{3/2}$	116 828*	($^3P_2$)15*p*
113 518*	$6p\ ^2D^o_{3/2}$	116 865*	($^3P_1$)17*p*
113 593*	$6p\ ^2D^o_{5/2}$	116 895*	($^3P_2$)16*p*
113 629*	$6p\ ^2P^o_{1/2}$	116 912*	($^3P_1$)18*p*
113 673*	$6p\ ^2P^o_{3/2}$	116 950*	($^3P_2$)17*p*
114 581*	$7p\ ^2D^o_{3/2}$	116 984*	($^3P_1$)20*p*
114 654*[b]	$7p\ ^2D^o_{5/2}/^2P^o_{1/2}$	116 995*	($^3P_2$)18*p*
114 660*[b]	$7p\ ^2D^o_{5/2}/^2P^o_{1/2}$	117 011*	($^3P_1$)21*p*
114 698*	$7p\ ^2P^o_{3/2}$	117 034*	($^3P_2$)19*p*
115 254*	$8p\ ^2D^o_{3/2}$	117 056*	($^3P_1$)23*p*
115 318*	$8p\ ^2P^o_{1/2}$	117 066*	($^3P_2$)20*p*
115 336*	$8p\ ^2D^o_{5/2}$	117 074*	($^3P_1$)24*p*
115 360*	$8p\ ^2P^o_{3/2}$	117 094*	($^3P_2$)21*p*
115 707*	$9p\ ^2D^o_{3/2}$	117 118*	($^3P_2$)22*p*
115 768*	$9p\ ^2P^o_{1/2}$	117 139*	($^3P_2$)23*p*
115 788*	$9p\ ^2D^o_{5/2}$	117 156*	($^3P_2$)24*p*
115 804*	$9p\ ^2P^o_{3/2}$		

[a]Assignments indicated with a prime refer to Rydberg states converging to the $^1D^e_2$ ionic state.

[b]The quantum defects of these two states are too close to reach a definitive assignment, especially because the quantum defects do not show a linear energy dependence due to the perturbing ($^1D^e_2$)3*p* Rydberg states.

$n=6$ and become appreciable in intensity above $n=8$.

From the quantum defects calculated for the newly observed energy levels it has been established that the $^2P^o_{1/2}$, $^2P^o_{3/2}$, and $^2D^o_{5/2}$ states converge to the $^3P^e_2$ ionic limit and the $^2D^o_{3/2}$ state converges to the $^3P^e_1$ ionic limit. Table III shows the convergence limits for the various series. The lowest ionization limit ($^3P^e_0$) of 117 225.66 cm^{-1} has previously been founded on that of $^3P^e_2$ by fitting the $(^3P^e)nd\ ^4F^e_{9/2}(n=3-6)$ and $nf\ G[5]^o_{11/2}$ energy levels, which are accurate to 0.001 cm^{-1}, to Ritz formulas [44,49]. The energy levels determined in the present study are only accurate to 2 cm^{-1}. Although there are now many more experimental energy levels available, because of the limited accuracy of the present data, no attempts were made to try to improve the previously determined ionization limits. As for the quartet states, the line positions observed for the $^2S^o_{1/2}$ Rydberg series are not listed, because for these weak lines the assignments are not always definitive. However, the ionization limits have been established from quantum defects (Table III). The $^4S^o_{3/2}$ and the $^4D^o_{7/2}$ quartet states are not observed in this study. The $^4D^o_{7/2}$ Rydberg series converges to the $^3P^e_2$ ionization limit, as this is the only limit that supports a $J=\frac{7}{2}$ component. The limit to which the $^4S^o_{3/2}$ Rydberg series converges can therefore also be deduced, as there is only one $J=\frac{3}{2}$ component left to be assigned. The limits for the $^4P^o_{5/2}$ and $^4D^o_{7/2}$ series reported previously [44] are in agreement with the present results. For high quantum numbers, the quantum defects show small deviations from a linear energy dependence, probably due to weak interactions between the Rydberg series. Because of the low accuracy (quantum defects become increasingly inaccurate as the ionization energy is approached) of the experimental results, these perturbations were not investigated.

For the principal quantum numbers $n=4-11$ most of the multiplet components of the np Rydberg series are observed as separate resonances in the wavelength scan. For higher quantum numbers Rydberg states converging to the same ionization limit are beginning to merge together (Fig. 2), and there are numerous accidental overlaps between the series converging to the different limits.

TABLE III. Convergence limits of the $(^3P^e_j)np$ Rydberg series $J_{ion}=0,1,2$.

Series	J_{ion}
$^2S^o_{1/2}$	0
$^4D^o_{3/2}$	0
$^4P^o_{1/2}$	1
$^4D^o_{1/2}$	1
$^4P^o_{3/2}$	1
$^2D^o_{3/2}$	1
$^4D^o_{5/2}$	1
$^2P^o_{1/2}$	2
$^4S^o_{3/2}$	2
$^2P^o_{3/2}$	2
$^2D^o_{5/2}$	2
$^4P^o_{5/2}$	2
$^4D^o_{7/2}$	2

For each of the three limits studied ($^3P^e_0$, $^3P^e_1$, and $^3P^e_2$), the highest observed principal quantum number is $n=24-25$. The two-photon absorption cross section in a Rydberg series is typically proportional to $(1/n^*)^3$. The experimentally observed drop in intensities is much more dramatic. At present, there is no explanation for this, although a change in the photodissociation cross section cannot be excluded. Certainly, the breakoff of the series cannot be due to field ionization, as very strong ($\sim$800 V/cm) electric fields are required to ionize $n=25$ Rydberg states. Magnetic-field effects have also been considered, as the field in the ionization region is quite strong ($\sim$1 T). The quadratic Zeeman effect will cause l mixing in high Rydberg states, and f character will be mixed into the p orbital (only wave functions of the same parity can mix). The photoionization matrix element will generally be much smaller for ionization of orbitals with high angular momentum (nonpenetrating orbitals). So, if a significant amount of f character is mixed in, the photoionization cross section will decrease dramatically. In recent experiments on Rb employing REMPI detection [50], it has been demonstrated that l mixing causes a breakoff in the intensity of transitions to a Rydberg series for $n>43$ in a magnetic field of 1 T. As the magnetic field in our experiments is also 1 T, and comparable states are accessed, it seems unlikely that the quadratic Zeeman effect can account for the breakoff of the Rydberg series already at $n<30$ in the present experiments. A second effect may be induced by the presence of the magnetic field. A particle moving in a magnetic field (**B**) with velocity **v** will experience an equivalent electric field with strength $\mathbf{E}=\mathbf{B}\times\mathbf{v}$[51]. The velocity of the N atom is estimated to be in the order of 4000 m/s, leading to an electric field of 40 V/cm. As mentioned above, much higher fields are required for field ionization of $n=25$ Rydberg states. It seems therefore unlikely that this effect can account for the present observations.

3. *Interloper states*

In the region below the first IE (14.534 eV above the ground state) there are only few states which belong to Rydberg series converging to an excited ionic state, namely the $^2F^o_J$, $^2P^o_J$, and $^2D^o_J$ states arising from the $(^1D^e_2)3p$ configuration, converging to the $^1D^e_2$ limit. The only other component of these series that has been re-

TABLE IV. Coefficients squared of the wave function $\Psi=c\phi((^3P^e)np)_{L,S,J}+d\phi((^1D^e)3p)_{L,S,J}$ determined in a (limited) MQDT analysis.

	$^2P^o_{1/2}$		$^2P^o_{3/2}$		$^2D^o_{3/2}$		$^2D^o_{5/2}$	
np	c^2	d^2	c^2	d^2	c^2	d^2	c^2	d^2
4	96	4	96	4	93	7	92	8
5	75	25	67	33	76	24	78	22
6	92	8	92	8	97	3	97	3
7	98	2	98	2	99	1	99	1
8	99	1	99	1	99	1	100	0
9	100	0	100	0	100	0	100	0
⋮								

ported is the $(^1D_2^e)4p\ ^2F^o$ state, at 122 246.4 cm^{-1} above the $^4S^o_{3/2}$ ground state [43]. This state, and all other $(^1D_2^e)np$ configurations, lies above the first E_i and outside the energy range studied. The $(^1D_2^e)3p$ interlopers strongly perturb the $(^3P_J^e)np$ Rydberg series around $n=5$ (Fig. 1) [49]. A limited MQDT analysis has been performed to assess the degree of mixing and hence the relative contributions of $(^3P_J^e)np$ and $(^1D_2^e)3p$ character in the wave functions. To limit the number of interacting channels, it is assumed that around $n=5$, L and S are still good quantum numbers and that only states of the same L, S, and J can interact. This reduces the problem to four ($^2P^o_{1/2}$, $^2P^o_{3/2}$, $^2D^o_{3/2}$, and $^2D^o_{5/2}$) two-channel MQDT analyses, resulting in wave functions of the following type:

$$\Psi_{L,S,J}=c\psi((^3P^e)np)_{L,S,J}+d\psi((^1D_2^e)3p)_{L,S,J}\ . \quad (1)$$

The results of these analyses are given in Table IV. The effective quantum numbers, and hence the presence of perturbations, of the $^2P^o_{3/2}$ Rydberg series relative to the $^3P_2^e$ and $^1D_2^e$ ionic limits are shown in a Lu-Fano plot (Fig. 3). The assumptions made are probably reasonable, as we know that LS coupling breaks down at $n\sim 7$, whereas at $n=5$, LS coupling should still be a reasonable approximation. Also, if states having the same total angular momentum but different L and S mix, the $(^1D_2^e)3p\ ^2F^o_{5/2}$ state will be perturbed by the $^2D^o_{5/2}$ states, whereas the $^2F^o_{7/2}$ state will be unperturbed. If this is the case, it will likely lead to differences in the photoelectron spectra for these two states. The observed photoelectron spectra are the same (*vide infra*), suggesting that only states having the same L and S interact.

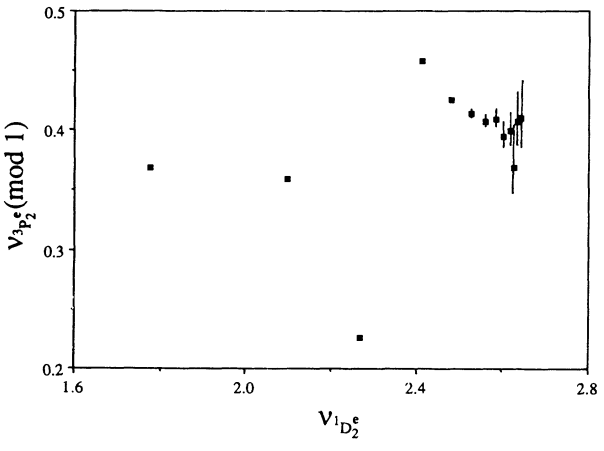

FIG. 3. Lu-Fano plot showing the interaction between the $^2P^o_{3/2}$ components of the $(^3P_2^e)np$ and $(^1D_2^e)3p$ Rydberg series. The symbol $\nu_{^3P_2^e}$ signifies the effective quantum number relative to the $^3P_2^e$ limit, $\nu_{^1D_2^e}$ the effective quantum number relative to the $^1D_2^e$ limit. Because of the increasing inaccuracy of the quantum defects, only principal quantum numbers from $n=3$ up to 15 are included in the figure.

TABLE V. Branching ratios observed in the PE spectra from the $^2D^o$ initial state via all observed intermediate states.

Initial state	Intermediate state	$^3P^e_{0,1,2}$ (%)	$^1D_2^e$ (%)
$^2D^o_{3/2}$	$3p\ ^2S^o_{1/2}$	100	0
$^2D^o_{5/2}$	$3p\ ^2S^o_{1/2}$	100	0
$^2D^o_{3/2}$	$3p\ ^2P^o_{3/2}$	89	11
$^2D^o_{5/2}$	$3p\ ^2P^o_{3/2}$	91	9
$^2D^o_{3/2}$	$3p\ ^2P^o_{1/2}$	91	9
$^2D^o_{5/2}$	$3p\ ^2P^o_{1/2}$	91	9
$^2D^o_{3/2}$	$3p\ ^2D^o_{5/2}$	92	8
$^2D^o_{5/2}$	$3p\ ^2D^o_{5/2}$	88	12
$^2D^o_{3/2}$	$3p\ ^2D^o_{3/2}$	91	9
$^2D^o_{5/2}$	$3p\ ^2D^o_{3/2}$	81	19
$^2D^o_{3/2}$	$4p\ ^2S^o_{1/2}$	100	0
$^2D^o_{5/2}$	$4p\ ^2S^o_{1/2}$	100	0
$^2D^o_{3/2}$	$4p\ ^2P^o_{3/2}$	84	16
$^2D^o_{5/2}$	$4p\ ^2P^o_{3/2}$	83	17
$^2D^o_{3/2}$	$4p\ ^2P^o_{1/2}$	80	20
$^2D^o_{5/2}$	$4p\ ^2P^o_{1/2}$	81	19
$^2D^o_{3/2}$	$4p\ ^2D^o_{5/2}$	82	18
$^2D^o_{5/2}$	$4p\ ^2D^o_{5/2}$	79	21
$^2D^o_{3/2}$	$4p\ ^2D^o_{3/2}$	84	16
$^2D^o_{5/2}$	$4p\ ^2D^o_{3/2}$	87	13

C. Photoelectron studies and ionic branching ratios

1. REMPI PES from the $^2D^o$ initial state

Photoelectron spectra were recorded for all the 20 observed transitions into the $3p$ and $4p$ Rydberg levels; the ionic state branching ratios are given in Table V. As mentioned, the splittings between the $J=0$, 1, and 2 components of the $^3P^e$ ionic state are not resolved due to a Doppler-type broadening of the PE signals of ~ 15 meV.

Only the ionic ground state is energetically accessible via the $(^3P^e)3p\ ^2S^o_{1/2}$ intermediate state at two-photon energies of 74 357 and 74 348 cm^{-1}, and so ions are produced in the $^3P^e$ ionic state with 100% selectivity as previously reported [35]. For the other states, ionization to the $^1D_2^e$ ionic state (15 319.19 cm^{-1} above the ground ionic state) [44] can also take place. Ionization of unperturbed Rydberg states should, in principle, occur with preservation of the ion core, so transitions to the $^3P^e$ ionic state should dominate. This is indeed observed; the $^3P^e_{0,1,2}$:$^1D_2^e$ branching ratios are approximately 1:0.2 for all of the multiplet components. As can be expected, the branching ratios are the same if the intermediate state is populated from the $^2D^o_{3/2}$ or $^2D^o_{5/2}$ initial states.

2. REMPI PES from the $^2P^o$ initial state

$(^3P^e)nf$ series. PE spectra were recorded only for the lower members of the nf series ($n=4$–6). For higher principal quantum numbers, the resonances are too weak to obtain adequate statistics. In the PE spectra only transitions to the $^3P^e$ ionic state have been discerned, even though energetically three ionic states are accessible. This high degree of core selectivity is probably due to the high orbital angular momentum ($l=3$) of the Rydberg electron, whose removal should not affect the core. So, when ionization occurs via members of the $(^3P^e)nf$ Rydberg

TABLE VI. Branching ratios observed in the PE spectra from the $^2P^o$ initial state. The transition to the $^1S_0^e$ ionic state is always very weak (< 5%) and is not included in the table.

	$^2P^o_{1/2}$		$^2P^o_{3/2}$		$^2D^o_{3/2}$		$^2D^o_{5/2}$	
np	$^3P^e$ (%)	$^1D^e$ (%)	$^3P^e$ (%)	$^1D^e$ (%)	$^3P^e$ (%)	$^1D^e$ (%)	$^3P^e$ (%)	$^1D^e$ (%)
4	91	9	91	9	88	12	92	8
5	71	29	48	52	48	52	58	42
6	71	29	64	36	74	26	77	23
7	85	15	72	28	86	14	85	15
8	83	17	78	22	86	14	93	7
9	87	13	77	23	89	11	92	8
10	92	8	72	28	85	15	94	6
11	94	6	81	19			92	8

series, state-selective production of ions in the electronic ground state is achieved.

$(^3P^e)np$ series. For (2+1) ionization from the $^2P^o_j$ metastable state, three ionic states ($^3P^e$, $^1D^e_2$, and $^1S^e_0$) are energetically accessible, except if ionization takes place via the $(^3P^e)3p$ and $(^3P^e)4p$ Rydberg states where only the lowest two ionic states are within reach. PE spectra have been recorded for most of the observed transitions, and the ionic state branching ratios are given in Table VI. When energetically permitted, transitions to the $^1S^e_0$ ionic state at 32 688.64 cm^{-1} above the ground ionic state [44] are very weak, at most a few percent of the total signal. For those intermediate states where the wave functions are perturbed by the $(^1D^e_2)3p$ interlopers (below), the transition to the $^1D^e_2$ ionic state is strongly enhanced, as can be expected. Typical PE kinetic-energy scans are shown in Figs. 4(a)–4(d) for photoionization to the 4*p*, 5*p*, 6*p*, and 10*p* Rydberg levels. The spacing between peaks of 1.90 and 2.15 eV provides the first electron spectroscopy measurement of the $N^+(^1D^e_2$-$^3P^e)$ and the $N^+(^1S^e_0$-$^1D^e_2)$ separations, respectively. These compare to the more accurately known values of 1.899 and 2.154 eV [44]. He I PES [52] has given the IE to the ground-state cation only, since the spin selection rule in *LS* coupling dictates that the singlet excited states of N^+ are formally forbidden using one-photon ionization from the $^4S^o_{3/2}$ ground state.

The branching ratios for transitions to the ionic states, determined by PES, can, in principle, be related to the coefficients squared in the wave functions of the Rydberg

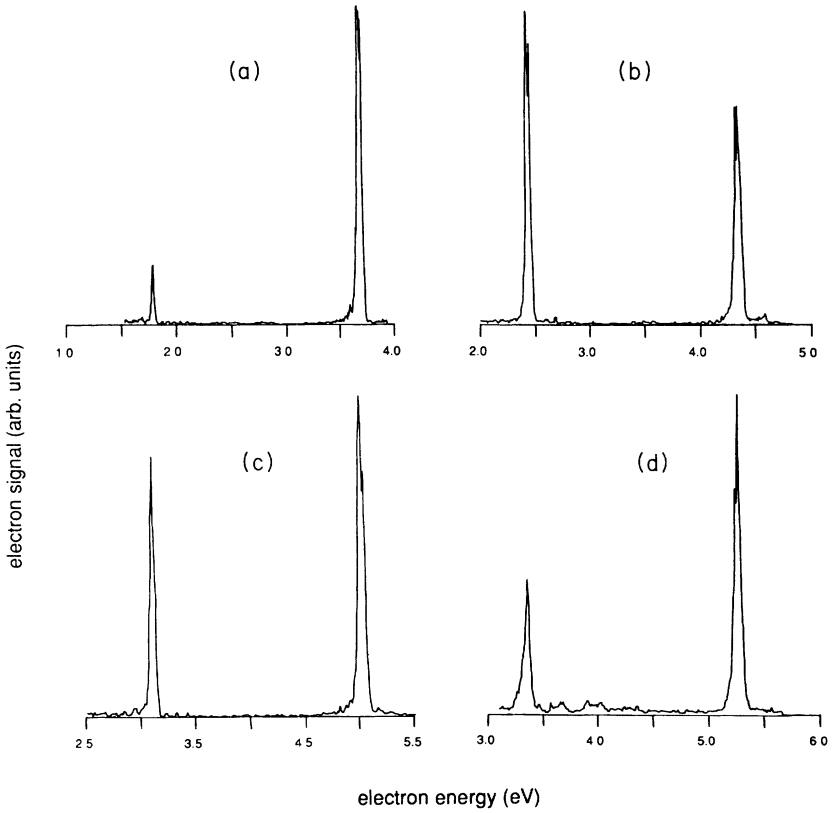

FIG. 4. Photoelectron kinetic-energy scans associated with ionization from the $^2P^o$ metastable state via the $^2P^o_{3/2}$ components of the $(^3P^e_2)np$ Rydberg states, with (a) $n=4$, (b) $n=5$, (c) $n=6$, and (d) $n=10$. The weak peak at low kinetic energy corresponding with the $^1S^e_0$ ionic state is not shown.

states determined from the MQDT analysis (Table IV). For transitions to the $^3P^e$ and $^1D_2^e$ ionic states the transition probabilities are proportional to

$$\left|\left\langle \Psi(^1D_2^e)\varepsilon l \left| \sum_j \mathbf{r}_j \right| c\psi((^3P^e)np) + d\psi((^1D_2^e)3p) \right\rangle\right|^2 \quad (2a)$$

and

$$\left|\left\langle \Psi(^3P^e)\varepsilon l \left| \sum_j \mathbf{r}_j \right| c\psi((^3P^e)np) + d\psi((^1D_2^e)3p) \right\rangle\right|^2 . \quad (2b)$$

A direct quantitative comparison, however, between the wave-function composition and the photoelectron branching ratios is not straightforward, since this analysis does not take into consideration the kinetic-energy dependence of the cross sections. In addition, Cooper minima are known to play a role in the (2+1) REMPI of $N(^2D_J^o)$ atoms via the $(^3P^e)3p$ Rydberg state [35–38]. As similar states and electron energies are accessed in the present experiments, Cooper minima are also likely to play a role here.

The PE spectrum for ionization via the $(^3P^e)4p\ ^2P_{3/2}^o$ level at a two-photon energy of 78 789 cm^{-1} is shown in Fig. 4(a), and indicates very little perturbation. This should be contrasted with the PE spectrum via the $(^3P^e)5p\ ^2P_{3/2}^o$ state which occurs at a two-photon energy of 82 374 cm^{-1} [Fig. 4(b)]. In this case the three lowest electronic states of the ion, the $^3P_{0,1,2}^e$, $^1D_2^e$, and $^1S_0^e$ states are all energetically accessible, with the transition to $^1S_0^e$ weakly observed. The $^3P_{0,1,2}^e$:$^1D_2^e$ intensity ratio of 0.94:1 is due to a strong perturbation by the $(^1D_2^e)3p$ state. This bound-bound interaction leads to appreciable energy shifts of up to $\sim$500 cm^{-1} [49] (see also Fig. 3) and strong mixing of wave functions. From the two-channel MQDT analysis the mixing coefficients $|c|=0.82$ and $|d|=0.57$ [Eq. (1)] are obtained, and the square of these should approximate to the experimental intensities with the reservations discussed above. This mixing with the wave function of the $(^1D_2^e)$ interloper is reflected in the experimentally observed ionic state branching ratios (Table VI) which show that the transition to the $^1D_2^e$ ionic state is strongly enhanced for all Rydberg wave functions having both $(^3P^e)np$ and $(^1D_2^e)3p$ character. Core switching of this type has been seen before in REMPI-PES of Xe [2,53,54] and other polyelectronic main group [55,56] and transition metal atoms [57–60].

To select an unperturbed situation, we will discuss ionization via a high Rydberg state, which is unaffected by interlopers. The $^1D_2^e$ intensity is seen to drop off at $6p$ [Fig. 4(c)], and this is tracked, in part, by the MQDT wave-function analysis. The PE for ionization via the $(^3P^e)10p\ ^2P_{3/2}^o$ intermediate state is shown in Fig. 4(d). The $^3P^e$:$^1D_2^e$ branching ratio is 1:0.2, and transition to the $^1S_0^e$ ionic state is not observed. The transition in which the ionic core is preserved dominates. This core preservation is observed, to a greater or lesser extent, up to the maximum n for which we have recorded PE spectra ($n=16$) when photoionization takes place via a nominally unperturbed $(^3P^e)np$ Rydberg state. The transition to the $^1D_2^e$ ionic state is still appreciable, however. The amount of core switching is observed to depend on the quantum numbers J, L, and S. When ionization occurs via unperturbed $^2P_{3/2}^o$ components of the $(^3P^e)np$ series, the $^3P_{0,1,2}^e$:$^1D_2^e$ branching ratios are roughly 1:0.2. However, the observed $^3P_{0,1,2}^e$:$^1D_2^e$ branching ratios for the unperturbed $^2P_{1/2}^o$, $^2D_{3/2}^o$, and $^2D_{5/2}^o$ intermediate states are approximately 1:0.1. This effect is probably due to a J, L, and S dependence of the photoionization matrix element and configuration interaction in the continuum.

$(^1D_2^e)3p$ interloper states. Those states that possess a $^1D_2^e$ ion core, not surprisingly, show the greatest intensity upon photoionization to the $^1D_2^e$ ion. Figures 5(a)–5(c)

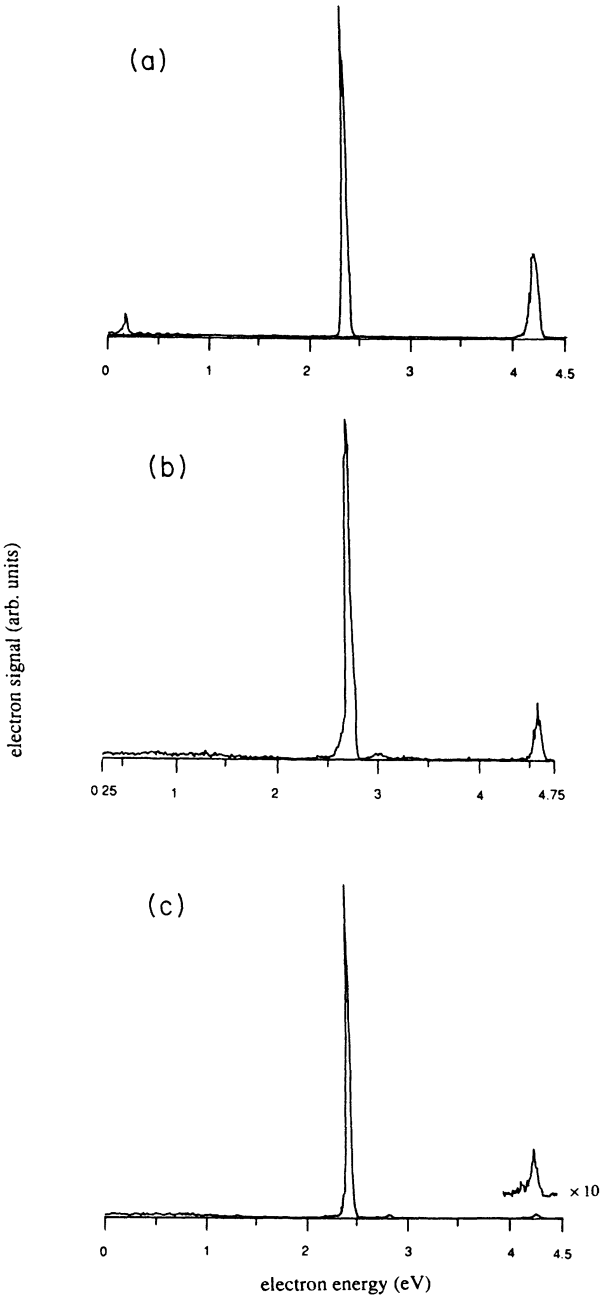

FIG. 5. Photoelectron kinetic-energy scans associated with ionization from the $^2P^o$ metastable state via the (a) $^2P_J^o$, (b) $^2D_J^o$, and (c) $^2F_J^o$ components of the $(^1D_2^e)3p$ interloper states.

show representative kinetic-energy scans for three sets of transitions originating from the $^2P_j^o$ metastable which access states with the $^1D_2^e$ core. In all cases the transition to the $^1D_2^e$ ionic state dominates. When photoionization of the N atom occurs via the unique $(^1D_2^e)3p\ ^2F_{5/2}^o$ Rydberg state, whose PE spectrum is depicted in Fig. 5(c), a very high degree of state selectivity is observed. A similar branching ratio is observed if ionization takes place via the $J=\frac{7}{2}$ component. From the ionic state branching ratios ($^3P_{0,1,2}^e:{}^1D_2^e=0.05:1$) we conclude that the $^2F^o(J=\frac{5}{2}$ and $\frac{7}{2})$ Rydberg states are hardly perturbed by the $(^3P^e)np$ Rydberg series. As already stated above, this supports our assumption that mixing only takes place between states having the same L, S, and J quantum numbers. Thus, when either the $(^1D_2^e)3p\ ^2F_{5/2}^o$ or $^2F_{7/2}^o$ state is selected in the REMPI process, N^+ ions are generated with high specificity ($>95\%$) in their electronically excited $^1D_2^e$ state. This state-selective production of electronically excited N^+ is very intriguing in view of the recent interest in state-selective chemistry.

D. Production of $N(^2D^o)$ and $N(^2P^o)$

At this stage, given that only one laser is used for both photolysis and detection, it is difficult to unambiguously establish a mechanism for the production of the $N(^2D^o)$ and $N(^2P^o)$ metastable states. Still, some worthwhile information can be deduced from the present experiments. It has been demonstrated previously that HN_3 has two primary dissociation channels in the uv region [5]:

$$HN_3(^1A')\rightarrow N_2(^1\Sigma_g^+)+NH(a\,^1\Delta)\ , \tag{3}$$

$$HN_3(^1A')\rightarrow N_3(^2\Pi_g)+H(^2S)\ . \tag{4}$$

Much research has focused on the characterization of the photofragmentation process described by Eq. (3), whereas much less is known about the other pathway, Eq. (4). Via reaction (3) NH is formed predominantly in its $a\ ^1\Delta$ state, with several vibrational levels populated [4–13]. At short wavelengths (<200 nm), other excited singlet states also are populated to some extent [7]. Reaction path (3) is found to be the dominant channel, but reaction (4) is not negligible. This is evidenced by the fact that in the present experiments a very strong signal is observed at 243.1 nm, which is associated with (2+1) REMPI of H atoms via the $n=2$ level. In Fig. 6 the wavelength scan, employing low laser power to avoid saturation, is depicted, showing a "Doppler-split" line shape. In principle, the observed H atoms can be formed either via reaction (4) or via photodissociation of $NH(a\ ^1\Delta)$. If $NH(a\ ^1\Delta)$ is considered as the precursor of H atoms, the accompanying N atom should be formed in a doublet state, the most likely candidates being $^2D^o$ and $^2P^o$. So, an analysis of the line shape of the $H(n=2)$ resonance can provide information not only on the origin of the hydrogen atom, but also on the origin of the metastable nitrogen atoms. A second possible pathway for formation of $N(^2D^o)$ and $N(^2P^o)$ is photodissociation of N_3. As in the case of the resonance line shape observed for the H atom, the Doppler broadening of the resonances observed for the N atom can provide information on the photodissociation

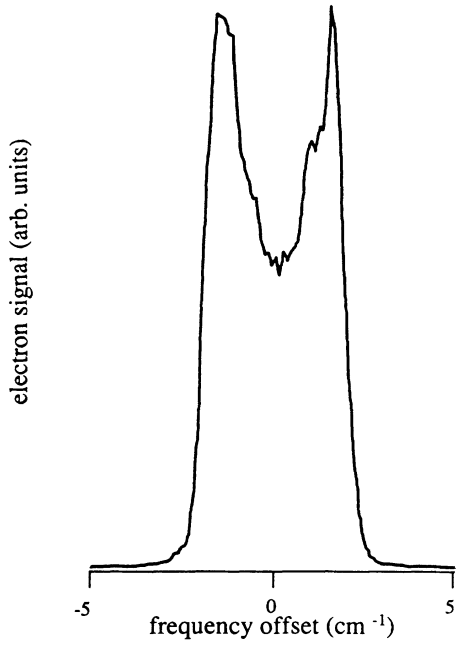

FIG. 6. Doppler profile of the H atom transition $^1S_0+e^-\leftarrow{}^2S^e,{}^2D^e\leftarrow\leftarrow{}^2S_{1/2}^e$ at 243.1 nm.

mechanism. The, albeit small, Doppler broadening is quite different for the two proposed dissociation mechanisms, i.e., photolysis of NH and N_3. The momentum conservation rule dictates that the lightest fragment formed in the dissociation process gains the highest velocity. This means that, for comparable excess energies, the velocity of N atoms formed from dissociation of N_3 (where N is the lighter fragment) is much greater than the velocity of N atoms formed from dissociation of NH (where the N fragment is by far the heaviest). In the following it will be demonstrated that the linewidth of the H atom resonance indicates that H atoms are most likely formed via reaction path (4). From the linewidths observed for N atom resonances, it is inferred that $N(^2D^o)$ and $N(^2P^o)$ are probably formed via photolysis of N_3.

The frequency of light absorbed by a system, which has a velocity component v_z relative to the propagation direction of the light, will be

$$\nu=\nu_0(1-v_z/c) \tag{5}$$

where ν_0 is the absorption frequency of the system at rest.

The doubly peaked shape of the Doppler broadened profile observed for the $H(n=2)$ resonance indicates that the majority of the H atoms have a high-velocity component along the laser propagation direction. Since the propagation is perpendicular to the polarization direction, the H atoms have an anisotropic translation perpendicular to the polarization. The angular distribution of the H atom for a single recoil velocity and linearly polarized light is given by [61]

$$W(\theta)=(1/4\pi)\{1+\beta P_2(\cos\theta)\}\ ,$$

where $P_2(x)=(3x^2-1)/2$ and θ is the angle between the

fragment recoil direction and the polarization of the light. The limiting values of the anisotropy parameter β are $+2$ and -1, corresponding to recoil along and perpendicular to the polarization vector, respectively, while $\beta=0$ corresponds to an isotropic angular distribution of the fragments. Doppler profiles predicted for $\beta=+2$, 0, and -1 are given in Figs. 7(a)–7(c). The observed profile for the H($n=2$) resonance, depicted in Fig. 6 is similar to situation (c), indicating fast fragmentation and a transition moment perpendicular to the laser polarization. From the profile a recoil velocity of the H fragment of 1.13×10^4 m/s is deduced, in perfect agreement with the value of 1.13×10^4 m/s, found for photolysis of HN_3 at 248 nm [62].

Let us now consider the possible dissociation pathways and associated recoil velocities. If photolysis of NH ($a\ ^1\Delta$) is considered at 243.1 nm, one-photon dissociation can energetically only take place to $H+N(^2D^o)$. As strong transitions from $N(^2P^o)$ are observed at approximately this wavelength, it seems unlikely that one-photon dissociation of NH is the sole origin of the atomic species observed. However, it cannot be excluded as a production mechanism for $H+N(^2D^o)$. The H atom recoil velocity for this process is 1.25×10^4 m/s, slightly larger than the value of 1.13×10^4 m/s deduced from the profile. If NH is photolyzed at the two-photon level, $H+N(^2D^o)$ and $H+N(^2P^o)$ give rise to H atom recoil velocities of 3.27×10^4 and 2.92×10^4 m/s, respectively, which would lead to significantly broader Doppler profiles (9 and 8 cm^{-1}). The second photolysis pathway is one-photon dissociation of HN_3, via Eq. (4). Here, the internal energy distribution of the N_3 fragment influences the recoil velocity of the H atom. The dissocation energy and internal energy of the N_3 fragment of this reaction are not known accurately, allowing only a crude estimate of the maximum H atom recoil velocity (assuming N_3 gains no internal energy) of $\sim1.2\times10^4$ m/s.

From the above discussion, we suggest that the H atoms are, most likely, formed from direct photodissociation of HN_3, in agreement with a previous study [62]. This implies that N_3 (or N_2+N) are effectively formed and N_3 has indeed been observed upon photolysis of HN_3 at 248 nm [62]. N_3 should then be considered as a possible precursor for the N metastable states. The absorption of N_3 is very diffuse for wavelengths <272 nm [63]. At 272 nm, and presumably also at shorter wavelengths, N_3 predissociates rapidly to form $N(^2D^o)+N_2(X)$ [63]. This is in line with the present results where transitions from $N(^2D^o)$ are only observed for wavelengths <272 nm. However, this in itself proves little as no resonances are to be expected from $N(^2D^o)$ at wavelengths between 290.3 and 272 nm. As mentioned previously, the resonances from $N(^2P^o)$ to the $(^3P^e)3p$ and $(^3P^e)4p$ states at ~290–294 and ~254 nm, are anomalously weak, indicating that photodissociation channels leading to $N(^2P^o)+N_2(X)$ are closed at these wavelengths and higher order processes are needed to produce $N(^2P^o)$. Photolysis of N_3 to $N(^2P^o)+N_2(X)$ can probably take place at shorter wavelengths.

Again, the Doppler broadening of the resonances can provide information on the origin of the N metastable states. If $N(^2D^o)$ is formed via one or two-photon dissociation of NH, Doppler widths of 0.24 and 0.77 cm^{-1} would be expected. If $N(^2D^o)$ is formed from N_3, the width depends on the internal energy of the N_2 fragment. If it is assumed that N_2 gains negligible internal energy, N resonances should have a width of 1.5 cm^{-1}. Analogously, a Doppler width of 0.6 cm^{-1} would be expected for resonances from the $N(^2P^o)$ metastable if generated via two-photon dissociation of NH. If $N(^2P^o)$ is generated via single-photon dissociation of N_3, a width of 1.2 cm^{-1} is expected. The observation linewidths of 1.35 and 1.2 cm^{-1} for transitions from $N(^2D^o)$ and $N(^2P^o)$, respectively, indicate that these species are probably formed via photolysis of N_3.

Two-color experiments where the N atom production is monitored for various dissociation wavelengths, together with theoretical investigations into the electronically excited states of N_3, are needed to substantiate these preliminary assignments.

IV. CONCLUSIONS

We have performed REMPI-PES measurements on many new doublet states of odd parity of the N atom, accessed by two-photon excitation from the $^2D_J^o$ and $^2P_J^o$ metastable states on N. Photodissociation of hydrazoic acid HN_3 proves to be a convenient source of N atom metastable states. The mechanism for the metastable atom production is probably via $N_3(^2\Pi_g)$ photodissocia-

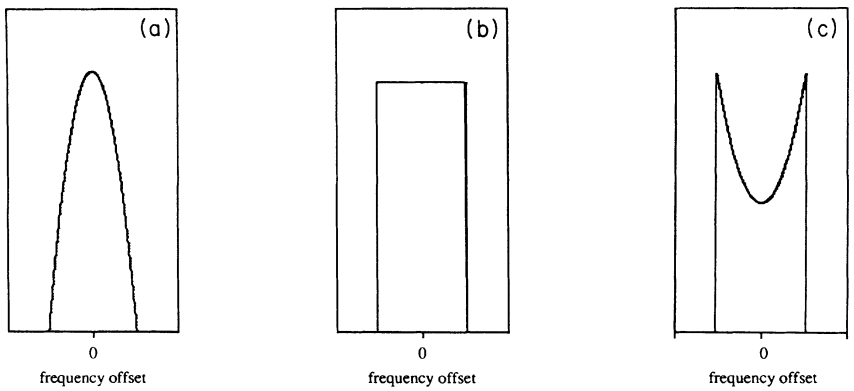

FIG. 7. Atomic Doppler profiles in the limiting cases (a) $\beta=2$, (b) $\beta=0$, and (c) $\beta=-1$.

tion. These species arise throughout the energy range considered via neutral channels, and the photodissociation cross section does not vary drastically with wavelength, except at the red end of the range studied, where transitions from the $^2P^o$ metastable state are anomalously weak.

The single-photon forbidden *np* and *nf* series have been observed between 88 100 and 117 500 cm^{-1}, and in the *np* case new states involving $n=6-25$ converging to the first IE have been observed. This provides new data on the higher Rydberg states of N atoms, and indicates a breakdown of *LS* coupling at high principal quantum numbers. Since photoionization of N occurs through high-lying Rydberg states with either a $^3P^e$ or $^1D_2^e$ core, photoelectron spectroscopy is a useful tool for determining branching ratios into the various ionic states. Both core-preserving and non-core-preserving transitions are observed. It is demonstrated that, by selecting specific intermediate states, ions can be generated with a high degree of state selectivity in the $^3P^e$ ground or the $^1D_2^e$ excited ionic state.

Future experiments must, in addition to establishing the photodissociation mechanism, address the important issue of photoionization cross sections for these excited states, of relevance to the predicted abundance of zeros in the $nl \rightarrow \varepsilon$, $l \pm 1$ dipole matrix elements (Cooper minima) for excited states of atoms [64–66]. Measurement of the photoelectron angular distributions, from which further information regarding the presence of Cooper minima may also be inferred, is clearly a worthwhile goal. In addition, experiments not much further to the blue will permit access to states above the first IE where autoionization processes should occur.

ACKNOWLEDGMENTS

E.d.B. and C.A.d.L. acknowledge the Netherlands Organization for Scientific Research (NWO) for equipment grants and financial support. N.P.C.W. thanks the Natural Sciences and Engineering Research Council of Canada, and the University of Guelph for grants in support of this work. The authors thank Dr. W. Vassen for assistance in performing the MQDT analysis and Dr. J. E. Hansen for helpful discussions.

*On leave from the Guelph-Waterloo Centre for Graduate Work in Chemistry, University of Guelph, Guelph, Ontario, Canada N1G 2W1.

[1] E. de Beer, M. Born, C. A. de Lange, and N. P. C. Westwood, Chem. Phys. Lett. **186**, 40 (1991).
[2] R. N. Compton and J. C. Miller, in *Laser Applications in Physical Chemistry,* edited by D. K. Evans (Dekker, New York, 1988).
[3] P. M. Dehmer, J. L. Dehmer, and S. T. Pratt, Comments At. Mol. Phys. **19**, 205 (1987).
[4] H. Okabe, J. Chem. Phys. **49**, 2726 (1968).
[5] H. Okabe, *Photochemistry of Small Molecules* (Wiley, New York, 1978).
[6] A. P. Baronavski, R. G. Miller, and J. R. McDonald, Chem. Phys. **30**, 119 (1978).
[7] F. Rohrer and F. Stuhl, J. Chem. Phys. **88**, 4788 (1988).
[8] J.-J. Chu, P. Marcus, and P. J. Dagdigian, J. Chem. Phys. **93**, 257 (1990).
[9] K.-H. Gericke, R. Theinl, and F. J. Comes, Chem. Phys. Lett. **164**, 605 (1989).
[10] K.-H. Gericke, R. Theinl, and F. J. Comes, J. Chem. Phys. **92**, 6548 (1990).
[11] H. H. Nelson and J. R. McDonald, J. Chem. Phys. **93**, 8777 (1990).
[12] K.-H. Gericke, T. Haas, M. Lock, R. Theinl, and F. J. Comes, J. Phys. Chem. **95**, 604 (1991).
[13] K.-H. Gericke, M. Lock, R. Fasold, and F. J. Comes, J. Chem. Phys. **96**, 422 (1992).
[14] R. D. Johnson and J. W. Hudgens, J. Chem. Phys. **92**, 6420 (1990).
[15] *Laser Probes for Combustion Chemistry, Vol. 134,* edited by D. R. Crosley (American Chemical Society, Washington, DC, 1980).
[16] A. N. Wright and C. A. Winkler, *Active Nitrogen* (Academic, New York, 1968).
[17] M. P. Iannuzzi and F. Kaufman, J. Chem. Phys. **73**, 4701 (1980).
[18] *Atoms in Astrophysics,* edited by P. G. Burke, W. B. Eissner, D. G. Hummer, and I. C. Percival (Plenum, New York, 1983).
[19] *Molecular Astrophysics,* edited by T. W. Hartquist (Cambridge University Press, Cambridge, 1990).
[20] D. E. Jennings, J. Quant. Spectrosc. Radiat. Transfer **40**, 211 (1988).
[21] M. J. Seaton, J. Phys. B **20**, 6363 (1987).
[22] P. M. Dehmer, J. Berkowitz, and W. A. Chupka, J. Chem. Phys. **60**, 2676 (1974).
[23] M. Le Dourneuf, V. K. Lan, and A. Hibbert, J. Phys. B **9**, L359 (1976).
[24] M. Le Dourneuf, V. K. Lan, and C. J. Zeippen, J. Phys. B **12**, 2449 (1979).
[25] C. J. Zeippen, M. Le Dourneuf, and V. K. Lan, J. Phys. B **13**, 3763 (1980).
[26] K. L. Bell and K. A. Berrington, J. Phys. B **24**, 933 (1991).
[27] C. M. Phillips, J. I. Steinfeld, and S. M. Miller, J. Phys. Chem. **91**, 5001 (1987).
[28] G. Black and L. E. Jusinski, Chem. Phys. Lett. **139**, 41 (1987).
[29] L. E. Jusinski, G. Black, and T. G. Slanger, J. Phys. Chem. **92**, 5977 (1988).
[30] C. P. Fell, J. I. Steinfeld, and S. M. Miller, Spectrochim. Acta **46A**, 431 (1990).
[31] L. E. Jusinski, G. E. Gadd, G. Black, and T. G. Slanger, J. Chem. Phys. **90**, 4282 (1989).
[32] A. Fujii and N. Morita, Chem. Phys. Lett. **182**, 304 (1991).
[33] J. C. Miller and W.-C. Cheng, J. Phys. Chem. **89**, 1647 (1985).
[34] J. Lavancier, D. Normand, C. Cornaggia, and J. Morellec, J. Phys. B **23**, 1839 (1990).
[35] S. T. Pratt, J. L. Dehmer, and P. M. Dehmer, Phys. Rev. A **36**, 1702 (1987).
[36] C. E. Theodosiou, Phys. Rev. A **37**, 1795 (1988).
[37] S. T. Manson, Phys. Rev. A **38**, 126 (1988).
[38] S. N. Nahar and S. T. Manson, Phys. Rev. A **40**, 5017 (1989).
[39] P. van der Meulen, E. de Beer, C. A. de Lange, N. P. C.

Westwood, and M. O. Krause, in *Synchrotron Radiation and Dynamic Phenomena, Grenoble, 1991,* edited by Alberto Beswick, AIP Conf. Proc. No. 258 (AIP, New York, 1992).
[40] B. G. Koenders, D. M. Wieringa, K. E. Drabe, and C. A. de Lange, Chem. Phys. **118**, 113 (1987).
[41] P. Kruit and F. H. Read, J. Phys. E **16**, 313 (1983).
[42] S. Bashkin and J. A. Stoner, *Atomic Energy Levels and Grotrian Diagrams, Vol. 1* (North-Holland, Amsterdam, 1975).
[43] C. E. Moore, *Atomic Energy Levels,* Natl. Bur. Stand. Ref. Data Ser., Natl. Bur. Stand. (U.S.) Circ. No. 35 (U.S. GPO, Washington, DC, 1971), Vol. 1.
[44] K. B. S. Eriksson, Phys. Scr. **34**, 211 (1986).
[45] R. D. Cowan and K. L. Andrews, J. Opt. Soc. Am. **55**, 502 (1965).
[46] M. J. Seaton, Proc. Phys. Soc. **88**, 801 (1966).
[47] U. Fano, J. Opt. Soc. Am. **65**, 979 (1975).
[48] M. J. Seaton, Rep. Prog. Phys. **46**, 167 (1983).
[49] K. B. S. Eriksson and J. E. Petterson, Phys. Scr. **3**, 211 (1971).
[50] L. D. Noordam, M. P. de Boer, and H. B. van Linden van den Heuvell, Phys. Rev. A **41**, 6267 (1990).
[51] C. W. Clark, K. T. Lu, and A. F. Starace, in *Progress in Atomic Spectroscopy (Part C),* edited by H. J. Beyer and H. Kleinpoppen (Plenum, New York, 1984), p. 247.
[52] J. Dyke, N. Jonathan, A. Morris, and T. Sears, J. Chem. Soc. Faraday Trans. 2 **72**, 597 (1976).
[53] R. N. Compton, J. C. Miller, A. E. Carter, and P. Kruit, Chem. Phys. Lett. **71**, 87 (1980).
[54] K. Sato, Y. Achiba, and K. Kimura, J. Chem. Phys. **80**, 57 (1984).
[55] S. T. Pratt, Phys. Rev. A **33**, 1718 (1986).
[56] J. Steadman and T. Baer, J. Chem. Phys. **89**, 5507 (1988).
[57] Y. Nagano, Y. Achiba, and K. Kimura, J. Chem. Phys. **84**, 1063 (1986).
[58] L. Sanders, A. D. Sappey, and J. C. Weisshaar, J. Chem. Phys. **85**, 6952 (1986).
[59] L. Sanders, S. D. Hanton, and J. C. Weisshaar, J. Chem. Phys. **92**, 3485 (1990).
[60] S. Niles, D. A. Prinslow, C. A. Wight, and P. B. Armentrout, J. Chem. Phys. **93**, 6186 (1990).
[61] M. N. R. Ashfold, I. R. Lambert, D. H. Mordaunt, G. P. Morley, and C. M. Western, J. Phys. Chem. **96**, 2938 (1992).
[62] K.-H. Gericke, M. Lock, and F. J. Comes, Chem. Phys. Lett. **186**, 427 (1991).
[63] R. Tian, J. C. Facelli, and J. Michl, J. Phys. Chem. **92**, 4073 (1988).
[64] A. Msezane and S. T. Manson, Phys. Rev. Lett. **35**, 364 (1975).
[65] A. Msezane and S. T. Manson, Phys. Rev. Lett. **48**, 473 (1982).
[66] J. Lahiri and S. T. Manson, Phys. Rev. Lett. **48**, 614 (1982).